The influence of hardener-to-epoxy ratio on the interfacial strength in glass fibre reinforced epoxy composites

Ross F. Minty, Liu Yang and James L. Thomason

University of Strathclyde, Department of Mechanical and Aerospace Engineering

Ross F. Minty, Liu Yang and James L. Thomason

University of Strathclyde, Department of Mechanical and Aerospace Engineering, 75 Montrose Street, Glasgow G1 1XJ, United Kingdom.

Abstract

This work seeks to develop a better understanding of the influence that the chemistry of an epoxy thermoset system has on the stress-transfer capability of the fibre-matrix interface. We discuss the correlation between the interfacial shear strength (IFSS) and the properties of the matrix such as glass transition temperature (T_g), storage modulus and linear coefficient of thermal expansion (LCTE). The results indicate that each is strongly dependent on the hardener-to-epoxy ratio and it was found that changes in IFSS can be related to changes in the thermomechanical properties of the matrix. From the results presented it is hypothesized that residual radial compressive stresses at the interface are influenced by the chemistry of the matrix system due to the changes in the properties of the matrix. The combination of these residual stresses with static friction may lead to a potential variation of the interfacial stress-transfer capability in glass-fibre reinforced epoxy composites.

Keywords: A Glass Fibres, B Fibre/matrix bond, B Interface/interphase, B Residual/internal stress.

1. Introduction

Over the past decades there has been a rapid growth in demand for, and development of, fibre-reinforced composite materials for use in high performance applications. At the same time, it has become increasingly clear that in order to continue optimizing performance then it will be necessary to better understand and measure the micro-mechanical parameters that control the structure-property relationships within such composites. Composite properties result from a combination of the material properties of the fibre and the matrix as well as the ability to transfer stresses across the fibre-matrix interface. Although tailoring the stress transfer capability is widely recognized as being vital to optimising the performance of the final composite, it is routinely reduced to a discussion about improving the 'adhesion' between the fibre and the matrix. Adhesion represents a simplified term for encompassing the multiple complex mechanisms that exist at the interface and contribute to its strength. One accepted mechanically measurable value for quantifying fibre-matrix adhesion is the apparent interfacial shear strength (IFSS).

Discussions about the interface in composites typically focus on the chemistry of the matrix system and the necessity to maximise the level of chemical bonding between the fibre and the matrix in order to optimize the level of 'adhesion' between the two [1–6]. However a number of authors have also commented on the potential role that shrinkage stresses may have in influencing the stress transfer capability of the interface[7–13]. Specifically, that residual radial compressive stresses (σ_R) formed at the interface may be a significant contributor to the measured strength of the interface. Thermal compressive radial stresses form during the cooling process due to differences in the thermal expansion coefficients of the matrix polymer and the reinforcement fibre. Thermosetting matrices also undergo volume change during polymerisation known as cure shrinkage. Due to the increase of the glass transition temperature (T_g) as thermoset matrix reacts and shrinks it is possible for some level of this

cure shrinkage to be ‘frozen’ into the system, creating additional residual stresses at the interface [14].

It is known that glass fibre sizings often utilise chemicals containing unreacted amine and epoxy groups to facilitate good adhesion between the glass fibre and epoxy matrix [15]. In practice however, the level of sizing applied to a coated fibre may also vary along the length of the fibre [15,16]. This has the potential to influence the amine: epoxy ratio at the interface and may lead to variations in the formation and performance of the fibre-matrix interface. Furthermore, there is a significant weight of opinion [14,17–20] that even if the residual stresses at the interface do contribute to the stress transfer capability, then chemistry and chemical reactions must also play an active role. Given these two important aspects in debate, it was considered necessary to study how they could be interrelated to influence the stress transfer capability of the interface. This work will build upon the findings reported in our previous study [8].

2. Experimental

2.1 Materials

Single boron free E-glass fibres coated with either γ-aminopropyltriethoxysilane (APS) or glycidoxypropyltrimethoxysilane (GPS) were taken from larger rovings supplied by Owens Corning-Vetrotex. The nominal tex was 1200 g/km and the average diameter was 17.5μm for both. Araldite® 506 epoxy resin and triethylenetetramine (TETA) were purchased from Sigma-Aldrich and used as received. The stoichiometric ratio for the system was calculated as 12.0% TETA. The ratios were varied from 4% TETA up to 30% TETA for the APS samples and 3.5% TETA up to 30% TETA for the GPS samples. This equated to an amine group: epoxy group ratio (R) varying from approximately 0.3 to 3.1 for both APS and GPS respectively. The resin mixtures, with different R values, were carefully measured and mixed

thoroughly before being degassed for approximated 15 minutes. Minute droplets of the resin mixture were then applied to a single glass fibre using a thin piece of steel wire. Approximately 60 droplets were placed on individual fibres before being transferred to a convection oven where they were heated to 60 °C, held isothermally for 1 hour and then further heated to 120 °C, being held isothermally for a further 2 hours. The heating rate was 2 °C/minute for both heating ramps and the samples were left to cool in the oven overnight. Prior to testing, all samples were examined under 200x magnification using a Nikon Epiphot inverted microscope to obtain values for the fibre diameter (D_f) and the fibre length (L_E) embedded in the resin droplet.

Samples for the differential scanning calorimetry (DSC), thermomechanical analysis (TMA) and dynamic-mechanical analysis (DMA) were prepared together, undergoing the same curing conditions that were used for the micro-droplet samples, with 9 different mixture ratios analysed. After de-gassing the epoxy resin was poured into a silicon mould and placed in a convection oven, producing 5 mm x 5 mm x 5 mm cubes for the TMA and 64 mm x 13 mm x 3 mm bars for the DMA. The DSC samples were produced by cutting unused TMA samples and shaping them into small flat discs. Samples bars for the near-infrared spectroscopy (nIR) were produced in the same manner to those for the DMA, with seven different R ratios studied.

2.2 Microbond Technique

The microbond technique is recognized as being a viable method for studying the apparent adhesion between the fibre and the polymer matrix via measurement of the IFSS [21]. This mechanically measurable value has been extensively used in past literature to quantify the strength of the interface between numerous fibres and polymer systems [7,8,22–25]. The apparatus for the test can vary greatly, with different methods for specimen clamping and

loading published in literature [26–31]. The configuration and development of the microbond test rig used in this study has been reported previously [26] and is shown in Figure 1. The rate of loading was maintained at 0.1 mm/s throughout the entire study. The load-displacement curve for each test was recorded in order to obtain a maximum force (F_{max}) at full interfacial de-bonding as shown in Figure 2. This value, along with the measured fibre diameter and embedded length, was used to estimate the apparent IFSS, τ_{app}, using Equation 1.

$$\tau_{app} = \frac{F_{max}}{\pi D_f L_e} \quad (1)$$

2.3 Thermomechanical Analysis

TMA was performed using a TA Q400 thermo-mechanical analyser, in combination with the cooling accessory MCA270 mounted with an expansion probe in accordance with ASTM standard E831-12. Experiments were conducted under a nitrogen flow of 50 ml/min. All samples were subjected to two heating runs from -10 to 150 °C at 10 °C/min. The cooling rate between the first and second run was -20 °C/min. The initial preload applied to the specimen was 0.1 N. DSC measurements were conducted using a TA Q20 DSC in combination with the cooling accessory RCS90 in accordance to ASTM standard E1356-08. A sample disc (15-20 mg) was weighed in small standard aluminium pans, sealed with an aluminium lid and the experiment was conducted under a nitrogen flow of 50 ml/min. All samples were subjected to two heating runs to account for thermal lagging, going from -10 to 150 °C at 10 °C/min. The cooling rate between the first and second run was -20 °C/min. DMA measurements were conducted using a TA Q800 dynamic-mechanical analyser in accordance to ASTM standard D5023-07. The analysis involved a 3-point bending test with rectangular shaped specimens held in place at either end whilst the centre underwent controlled oscillation, measuring the epoxy polymer's viscoelastic properties under flexure. All samples were subjected to one heating run, going from 30 to 150 °C at 2 °C/min. The

displacement amplitude was programmed to be 50 μm and the frequency was set at 0.1 Hz. The specimen was preloaded with a small force of 0.1 N.

2.4 Fourier Transform Infrared Spectroscopy

Fourier transform infrared spectroscopy (FT-IR) is a widely recognized technique used to obtain the infrared spectrum of emission or absorption of a material [32–36]. These spectra allow for the molecular structure of the material to be studied. Near-infrared (nIR) spectroscopy was used to analyse different R ratios due to its ability to allow for quantification of amine groups within the matrix. The nIR spectra were recorded in transmission using an ABB MB160.

2.5 Scanning Electron Microscopy

Analysis of de-bonded droplets was carried out using a Hitachi SU6600 scanning electron microscope (SEM), with an example shown in Figure 3. A small portion of the droplet is shown to have broken away and remained in the original position of the droplet prior to de-bonding. This portion is known as the meniscus. In order to ensure accuracy of the results the size of the remaining meniscus was measured and subtracted from the original measured embedded length value for each droplet to give the effective embedded length of the droplet before de-bonding. This in turn, was used to correct the IFSS value for each sample.

3. Results and discussion

3.1 Effect of amine:epoxy ratio on thermomechanical properties of the matrix

Thermal analysis was conducted in order to study thermomechanical properties of the matrix material such as the matrix linear coefficient of thermal expansion (LCTE), glass transition temperature (T_g) and matrix storage modulus. These properties are fundamentally dependent on molecular structure of the polymer and can be significantly affected by epoxy matrix R ratio. Figure 4 shows a plot of normalised dimension change versus temperature for a

selected number of the different ratios using the TMA. This plot allows for the evaluation of the T_g and LCTE values above and below T_g using the gradients of the curve at that point. It is shown in Figure 4 that as the ratio deviates further from the stoichiometric value of R = 1.0, the rate of dimension change will increase at the same temperatures. Figures 5 and 6 show the values for the LCTE above and below T_g plotted against R respectively. In both cases the LCTE is shown to be influenced by the chemistry of the system. Above T_g, the matrix is shown to possess the smallest LCTE value at the stoichiometric value, with the LCTE values increasing as the ratio deviates from stoichiometry. Below T_g a maximum is shown at around R = 0.5 before levelling out at the stoichiometric point and remaining fairly constant as more hardener was applied. The results in Figure 5 are expected since the maximum density of crosslinks in the molecular structure will form at the stoichiometric value [37]. Figure 6 illustrates that at low temperatures, there does not appear to be significant variation in the LCTE value apart from at a ratio of $R \approx 0.5$.

Figure 7 shows DSC normalised heat flow versus temperature plots for several of the different R ratios. It can be seen that a distinct drop in T_g occurred for R ratios with both excess epoxy and excess hardener respectively. Figure 8 shows the average values for T_g as the R ratio was varied. A maximum is observed slightly above the stoichiometric point, in the range of $1.1<R<1.3$. A clear correlation can be seen between the results produced by each of the techniques. For each data set, T_g tends to decrease as the R value deviates from the stoichiometric ratio. Figure 9 presents the DMA storage modulus of the matrix against temperature. It is shown that the epoxy modulus at stoichiometric ratio has the maximum values compared to the other ratios. At each temperature, the matrix modulus decreases as the ratio deviates further from the stoichiometric value. It is also noticed that excess epoxy ratios ($R < 1$) appears to cause more modulus reduction compared to that in the case of excess hardener ($R > 1$).

3.2 Effect of amine:epoxy ratio on IFSS

The results for the IFSS versus R ratio are shown in Figure 10. It can be seen that the IFSS values are clearly influenced by the R ratio for both silanes. Both sets of data show a strong correlation with each other, particularly at the extreme ratio values. A maximum in IFSS is shown to occur near the stoichiometric value (R = 1) for the APS sized fibres. For these samples it is clear that moving away from the stoichiometric ratio in either direction results in reduced IFSS, with a sudden drop in the IFSS when $R < 0.5$. For $0.5<R<2$ the changing ratio causes relatively small variations in the IFSS. For the GPS fibres a maximum is shown to occur at a ratio below the stoichiometric value ($R \approx 0.6$) before decreasing as the ratio deviated from this value. It is noticed that IFSS seems to drop faster for both silanes when there is a large excess of epoxy when compared to ratios with excess amine.

The results in Figure 8 and Figure 10 show that there is a strong correlation between the IFSS of the APS fibres and the T_g of the epoxy matrix. In both cases, the maximum value occurred near the stoichiometric point and these properties decrease as the R ratio deviated from this ideal ratio. Of particular interest is both T_g and IFSS drop away steeply at $R<0.5$. The similar effect of mix ratio on the T_g and the IFSS suggests a linear relationship between them. Figure 11 presents a plot of IFSS against T_g and it shows indeed that there seems to be a strong linear dependence of IFSS on the matrix T_g.

The dependence of the IFSS with the R ratio may be explained by chemical bonding to some degree [3,38,39]. For ratios containing excess epoxy ($R<1$), due to the lack of amine in the polymer system, it would be expected that more reactive epoxy groups would be available to bond with the reactive amine groups provided by the silane. This would create more covalent bonds across the interface. However, the lack of amine would also lead the system to be unable to form a full-crosslinked network. This would result in less restrained, bulky groups

forming at the end of epoxidic chain, increasing polymer free volume and decreasing key mechanical properties of the matrix [40–42]. The sudden drastic drop shown at $R < 0.5$ may represent a critical point where there were not enough reactive amine groups within the matrix system to produce a strong crosslinked structure. This would leave significant levels of unreacted epoxy groups.

To investigate this, near-infrared analysis (nIR) was conducted on cured samples of the epoxy system with different R ratios. This allowed for quantitative analysis of the unreacted components left within the matrix system after curing. An excess of unreacted epoxy groups is shown by the downward peak at 4530 cm^{-1} [34] in Figure 12 for samples where $R < 1.0$. For ratios with excess amine ($R > 1$), the reactive epoxy groups would statistically be less likely to bond with the amines provided by the silane due to the abundance of free primary amines already present within the matrix system, thus resulting in fewer bonds forming across the interface. For these ratios the curing reaction would also be dominated by the primary amines, with little secondary amine bonding, resulting in a more branched polymer matrix structure. This would result in significant levels of unreacted secondary amines within the system. nIR was used to confirm this as shown by the downward peak at 6460 cm^{-1} [34] in Figure 13, with the peak increasing as R increased. Depending on the R ratio it was also possible to have unreacted primary amine within the matrix as shown by the downward peak in Figure 14. This abundance of unreacted molecules as well as the branched structure would increase the polymer free volume due to the poor packing ability of the amine molecule, again leading to a decrease in the T_g [43,44]. However, we would expect the negative gradient of the IFSS curve to be larger for $R > 1$ than for $R < 1$, since in theory the number of bonds formed at the interface would be expected to drop as more amine was added to the system. Yet Figure 10 shows this to not be the case, with performance for $R > 1$ shown to maintain higher values for IFSS than for $R < 1$ for both silanes. This suggests that the R ratio

may also influence other adhesion mechanisms. The instance of a γ-APS coated fibre producing a strong interface under conditions where chemical bonding through the amino group should not be optimized has been discussed before, suggesting that there are indeed other significant adhesion mechanisms contributing to the IFSS [45].

Another potential explanation is that the residual radial compressive stresses (σ_R) formed during the curing process are being influenced by the properties of the matrix. For instance, the decrease in the modulus of the matrix and T_g shown in Figures 8 and 9 would lead to less residual stress at the interface. It was felt necessary to study this hypothesis to confirm its accuracy.

3.3 Effect of amine:epoxy ratio on residual thermal stress

Several models have previously been proposed [9–13] to quantify the formation of the thermal residual stresses at the interface due to differences in the coefficients of expansion of the matrix and fibre. Nairn [9] proposed a model to calculate the σ_R that accounted for the effects of differences in the axial and transverse fibre properties:

$$\sigma_R = A_1\left(1 - \frac{b^2}{r^2}\right) \tag{2}$$

where A_1 is the result of the calculation shown in Equation 3.

$$A_1 = \begin{bmatrix} X_{11} & X_{12} \\ X_{21} & X_{22} \end{bmatrix}\begin{bmatrix} A_1 \\ A_3 \end{bmatrix} = \begin{bmatrix} (\alpha_m - \alpha_{fT})\Delta T \\ (\alpha_m - \alpha_{fL})\Delta T \end{bmatrix} \tag{3}$$

Of the variables presented, b is a function of the fibre volume ratio (V_f), r is the radius of the fibre, α is the linear coefficient of thermal expansion, ΔT represents the difference between the stress-free temperature (T_s) and the testing temperature (T_t) and f, m, L and T are subscripts for the fibre, matrix, longitudinal and transverse respectively. From the result of the model in Equation 3 we can see that thermal residual stresses are directly influenced by

changes in ΔT. For thermosetting systems, the stress-free temperature is accepted as being the glass transition temperature T_g and hence the results for T_g presented in Figure 8 indicate that the level of residual stress should vary with the chemistry of the system as well as the testing temperature. Other key variables such as the matrix modulus and linear expansion coefficient of the matrix are also clearly dependent on both temperature and matrix chemistry as shown in Figures 4-6. Glass fibre properties are also temperature dependent, but to a much lesser degree, and can be considered constant for the temperature range explored in this study, with $\alpha_f = 6.0 \times 10^{-6}$ °C^{-1} used throughout this study [8].

Using Equation 3 and the above data, the magnitude of the interfacial radial thermal residual compressive stresses at room temperature were calculated for different ratios. These values were then used in Equation 4 with a coefficient of static friction coefficient of $\mu_s = 0.6$ [8,46] to obtain the residual stress contribution to the interfacial stress transfer capability (τ_R). The results are plotted in Figure 15.

$$\tau_R = \mu\sigma_R \quad (4)$$

It can be seen that as hardener was added to the epoxy system, the thermal stress contribution value changed, with a peak occurring at the stoichiometric point. Notably as the ratio deviated further from the stoichiometric value this contribution value was shown to decrease in a similar manner to that shown for the IFSS value in Figure 10. This correlation is expanded upon in Figure 16, where the IFSS value is plotted against the respective thermal residual stress contribution. We can see that similar to Figure 11, as the level of thermal residual stress at the interface was increased, the IFSS also increased. However, despite the clear correlation shown in Figure 16 we can see that this contribution by the thermal residual stresses still only represents about 20% of the final IFSS value. The slight decreases in IFSS shown in Figure 10 for R > 0.5 may possibly be attributed to the decrease in size of the

thermal residual stresses shown in Figure 15. For R < 0.5 it appears that multiple adhesion mechanisms must be influenced. As previously discussed the lack of amine at low R values may prevent the formation of a strong crosslinked structure thus resulting in a notable drop in performance for multiple thermomechanical properties associated with the strength of the interface. Another potential contributing factor may be the variation in residual stresses formed during the curing process due to the chemical curing reaction. These stresses are known as cure shrinkage stresses. Cure shrinkage is known to occur during the thermoset reaction process, however residual stress only builds up for the cure shrinkage which occurs after gelation due to the polymer structure becoming increasingly rigid, resulting in the stresses being unable to relax away [8,14,17,47,48]. Thus, there is potential for different levels of residual stress due to cure shrinkage forming during the curing process. It has been suggested in the past that residual cure shrinkage stresses may contribute significantly more than residual thermal stresses [8,14] and thus any changes in cure shrinkage stresses may significantly impact the stress transfer capability of the interface. This is the focus of another paper in preparation. Another point for future study will be to investigate the influence of the R ratio on the fracture toughness of the matrix. Fracture toughness, combined with interfacial adhesion, has a profound effect on the nature of fibre pull-out and as such is relevant to fully understanding the role of the R ratio in defining the properties of the interface.

In practice, the findings discussed in this paper highlight that poor mixing at the sub-micron level may lead to local variation of important matrix properties such as T_g and LCTE along the entire length of the fibre. This would change the performance of the interface and as such the final composite performance as well. Furthermore, the potential for local changes in the R ratio due to differences in the level of sizing applied to the fibre, along with its formulation, would clearly influence the formation and magnitude of the residual stresses located at the interface. Based on the results presented, this could significantly affect the stress transfer

capability of the interface if the R ratio deviated significantly from the stoichiometric value. This would suggest that sizings may play a broader role than promoting chemical bonding and protecting the fibre surface.

4. Conclusions

The results presented in this paper illustrate that the hardener-to-epoxy ratio can clearly influence multiple thermomechanical properties associated with defining the strength of the interface. The values for the IFSS, T_g, storage modulus and LCTE were shown to all be significantly influenced by the chemistry of the amine cured matrix, with notable drops in performance shown for each property when there was large degree of excess epoxy or excess amine in the system. Overall, the variation in these properties was taken as support for the hardener-to-epoxy ratio potentially not only influencing the level of chemical bonds forming between the fibre and matrix but also the formation of thermal residual radial compressive stresses located at the interface. It was shown that these residual stresses were influenced by the hardener-to-epoxy ratio and correlated with the values for IFSS, decreasing in size as the chemistry of the matrix deviated further from the stoichiometric value. However, the contribution of these thermal stresses represented only a small portion of the interface strength and cannot explain the sharp drop noted for excess epoxy ratios where $R < 0.5$. It is suggested that a larger residual stress contribution to the IFSS in these systems could be provided by the continued cure shrinkage of the matrix after gelation. One practical conclusion from the results presented here is that performance of the interface in thermoset composites is strongly related to the chemistry of the polymer matrix adjacent to that interface. Fibre sizings typically contain chemical reactive groups similar to the polymer matrices in their composites. Hence it is also possible that key interface properties of a glass fibre-reinforced epoxy composite may vary along the entire length of the embedded fibre. Small changes may result in small variations in the level of adhesion with minimum impact

on performance. However, if the variation from the stoichiometric value is large enough then there may be potential for a significant impact on performance of the final composite material.

Acknowledgements

The authors gratefully acknowledge the support of the Engineering and Physical Sciences Research Council (EPSRC). We would also like to thank the Advanced Material Research Laboratory (AMRL) and the Centre for Processing and Control Technology (CPACT) at the University of Strathclyde for use of their equipment and aid with the infrared spectroscopy respectively.

References

[1] Broutman LJ. Measurement of the Fiber-Polymer Matrix Interfacial Strength. Interfaces Compos ASTM STP 452 1969:27–41.

[2] Dey M, Deitzel JM, Gillespie JW, Schweiger S. Influence of sizing formulations on glass/epoxy interphase properties. Compos Part A Appl Sci Manuf 2014;63:59–67. doi:10.1016/j.compositesa.2014.04.006.

[3] Drzal LT, Madhukar M. Fibre-matrix adhesion and its relationship to composite mechanical properties. J Mater Sci 1993;28:569–610. doi:10.1007/BF01151234.

[4] Gray RJ, Johnston CD. The effect of matrix composition on fibre/matrix interfacial bond shear strength in fibre-reinforced mortar. Cem Concr Res 1984;14:285–96. doi:10.1016/0008-8846(84)90116-9.

[5] Jones FR. A Review of Interphase Formation and Design in Fibre-Reinforced Composites. vol. 24. 2010. doi:10.1163/016942409X12579497420609.

[6] Plonka R, Mäder E, Gao SL, Bellmann C, Dutschk V, Zhandarov S. Adhesion of epoxy/glass fibre composites influenced by aging effects on sizings. Compos Part A Appl Sci Manuf 2004;35:1207–16. doi:10.1016/j.compositesa.2004.03.005.

[7] Thomason JL, Yang L. Temperature dependence of the interfacial shear strength in glass-fibre polypropylene composites. Compos Sci Technol 2011;71:1600–5. doi:10.1016/j.compscitech.2011.07.006.

[8] Thomason JL, Yang L. Temperature dependence of the interfacial shear strength in glass-fibre epoxy composites. Compos Sci Technol 2014;96:7–12. doi:10.1016/j.compscitech.2014.03.009.

[9] Nairn JA. Thermoelastic analysis of residual stresses in unidirectional, high-performance composites. Polym Compos 1985;6:123–30. doi:10.1002/pc.750060211.

[10] Raghava RS. Thermal expansion of organic and inorganic matrix composites: A

Review of theoretical and experimental studies. Polym Compos 1988;9:1–11. doi:10.1002/pc.750090102.

[11] Wagner HD, Nairn JA. Residual thermal stresses in three concentric transversely isotropic cylinders: application to composites containing a interphase. Compos Sci Technol 1997;57:1289–302. doi:10.1016/S0266-3538(97)00058-4.

[12] Di Landro L, Pegoraro M. Carbon fibre thermoplastic matrix adhesion. J Mater Sci 1987;22:1980–6. doi:10.1007/BF01132927.

[13] Biro DA, Pleizier G, Deslandes Y. Application of the microbond technique: Effects of hygrothermal exposure on carbon-fiber/epoxy interfaces. Compos Sci Technol 1993;46:293–301. doi:10.1016/0266-3538(93)90163-B.

[14] Jakobsen J, Jensen M, Andreasen JH. Thermo-mechanical characterisation of in-plane properties for CSM E-glass epoxy polymer composite materials – Part 1: Thermal and chemical strain. Polym Test 2013;32:1350–7. doi:10.1016/j.polymertesting.2013.08.010.

[15] Thomason JL. Glass Fibre Sizings: A Review of the Scientific Literature. Blurb Inc; 2012.

[16] Thomason JL, Adzima LJ. Sizing up the interphase: An insider's guide to the science of sizing. Compos Part A Appl Sci Manuf 2001;32:313–21. doi:10.1016/S1359-835X(00)00124-X.

[17] Di Landro L, Pegoraro M. Evaluation of residual stresses and adhesion in polymer composites. Compos Part A Appl Sci Manuf 1996;27:847–53. doi:10.1016/1359-835X(96)00046-2.

[18] Chekanov YA, Korotkov VN, Rozenberg BA, Dhzavadyan EA, Bogdanova LM. Cure shrinkage defects in epoxy resins. Polymer (Guildf) 1995;36:2013–7. doi:10.1016/0032-3861(95)91446-E.

[19] Ismail H, Shuhelmy S, Edyham MR. The effects of a silane coupling agent on curing characteristics and mechanical properties of bamboo fibre filled natural rubber composites. Eur Polym J 2002;38:39–47. doi:10.1016/S0014-3057(01)00113-6.

[20] Ramos JA, Pagani N, Riccardi CC, Borrajo J, Goyanes SN, Mondragon I. Cure kinetics and shrinkage model for epoxy-amine systems. Polymer (Guildf) 2005;46:3323–8. doi:10.1016/j.polymer.2005.02.069.

[21] Miller B, Muri P, Rebenfeld L. A microbond method for determination of the shear strength of a fiber/resin interface. Composites 1987;18:267. doi:10.1016/0010-4361(87)90471-X.

[22] Ramanathan T, Bismarck A, Schulz E, Subramanian K. Investigation of the influence of acidic and basic surface groups on carbon fibres on the interfacial shear strength in an epoxy matrix by means by single-fibre pull-out test. Compos Sci Technol 2001;61:599–605. doi:10.1016/S0266-3538(00)00239-6.

[23] Liu B, Liu Z, Wang X, Zhang G, Long S, Yang J. Interfacial shear strength of carbon fiber reinforced polyphenylene sulfide measured by the microbond test. Polym Test 2013;32:724–30. doi:10.1016/j.polymertesting.2013.03.020.

[24] Li Y, Pickering KL, Farrell RL. Determination of interfacial shear strength of white rot fungi treated hemp fibre reinforced polypropylene. Compos Sci Technol 2009;69:1165–71. doi:10.1016/j.compscitech.2009.02.018.

[25] Wu GM, Shyng YT. Surface modification and interfacial adhesion of rigid rod PBO fibre by methanesulfonic acid treatment. Compos Part A Appl Sci Manuf 2004;35:1291–300. doi:10.1016/j.compositesa.2004.03.023.

[26] Yang L, Thomason JL. Development and application of micromechanical techniques for characterising interfacial shear strength in fibre-thermoplastic composites. Polym Test 2012;31:895–903. doi:10.1016/j.polymertesting.2012.07.001.

[27] Wada A, Fukuda H. Microbond Test for the Fiber/Matrix Interfacial Shearing Strength. 12th Int. Conf. Compos. Mater., Paris: 1999, p. 1–8.

[28] Morlin B, Czigany T. Cylinder test: Development of a new microbond method. Polym Test 2012;31:164–70. doi:10.1016/j.polymertesting.2011.10.007.

[29] Liu Z, Yuan X, Beck AJ, Jones FR. Analysis of a modified microbond test for the measurement of interfacial shear strength of an aqueous-based adhesive and a polyamide fibre. Compos Sci Technol 2011;71:1529–34. doi:10.1016/j.compscitech.2011.06.001.

[30] Craven JP, Cripps R, Viney C. Evaluating the silk/epoxy interface by means of the Microbond Test. Compos Part A Appl Sci Manuf 2000;31:653–60. doi:10.1016/S1359-835X(00)00042-7.

[31] Wang H, Wang H, Li W, Ren D, Yu Y. An improved microbond test method for determination of the interfacial shear strength between carbon fibers and epoxy resin. Polym Test 2013;32:1460–5. doi:10.1016/j.polymertesting.2013.09.017.

[32] Mertzel E, Koenig JL. Application of FT-IR and NMR to Epoxy Resins. Epoxy Resins Compos II 1985;75:74–112. doi:10.1007/BFb0017915.

[33] Lachenal G, Pierre A, Poisson N. FT-NIR spectroscopy: Trends and application to the kinetic study of epoxy/triamine system (Comparison with DSC and SEC results). Micron 1996;27:329–34. doi:10.1016/S0968-4328(96)00022-4.

[34] González-González M, Cabanelas JC, Baselga J. Applications of FTIR on Epoxy Resins - Identification, Monitoring the Curing Process, Phase Separation and Water Uptake. Infrared Spectrosc. – Mater. Sci. Eng. Technol., vol. 2, InTech; 2012, p. 261–84. doi:10.5772/2055.

[35] Meyer F, Sanz G, Eceiza A, Mondragon I. The effect of stoichiometry and thermal history during cure on structure and properties of epoxy networks. Polymer (Guildf)

1995;36:1407–14. doi:10.1016/0032-3861(95)95918-Q.

[36] Halvorson RH, Erickson RL, Davidson CL. The effect of filler and silane content on conversion of resin-based composite. Dent Mater 2003;19:327–33. doi:10.1016/S0109-5641(02)00062-3.

[37] Palmese GR, McCullough RL. Effect of epoxy-amine stoichiometry on cured resin material properties. J Appl Polym Sci 1992;46:1863–73. doi:10.1002/app.1992.070461018.

[38] Vanlandingham MR, Eduljee RF, Gillespie Jr. JW. Relationships between stoichiometry, microstructure, and properties for amine-cured epoxies. J Appl Polym Sci 1999;71:699–712. doi:10.1002/(sici)1097-4628(19990131)71:5<699::aid-app4>3.0.co;2-d.

[39] D'Almeida JRM, de Menezes WG, Neves Monteiro S. Ageing of the DGEBA / TETA Epoxy System with off-Stoichiometric Compositions 2 . Experimental Methods And Materials. Mater Res 2003;6:415–20. doi:10.1590/S1516-14392003000300017.

[40] D'Almeida JRM, Monteiro SN. Role of the resin matrix/hardener ratio on the mechanical properties of low volume fraction epoxy composites. Adv Perform Mater 1997;4:285–95. doi:10.1023/A:1008625121464.

[41] Bignotti F, Pandini S, Baldi F, De Santis R. Effect of the Resin/Hardener Ratio on Curing, Structure and Glass Transition Temperature of Nanofilled Epoxies Fabio. Polym Compos 2011;32:1034–48. doi:10.1002/pc.

[42] Li YF, Xiao MZ, Wu Z, Peng K, Han CM, Xiang W, Dai JY. Effects of epoxy/hardener stoichiometry on structures and properties of a diethanolamine-cured epoxy encapsulant. IOP Conf Ser Mater Sci Eng 2016;137:012012. doi:10.1088/1757-899X/137/1/012012.

[43] Calventus Y, Montserrat S, Hutchinson JM. Enthalpy relaxation of non-stoichiometric

epoxy-amine resins. Polymer (Guildf) 2001;42:7081–93. doi:10.1016/S0032-3861(01)00133-1.

[44] Kong F-M, Walkup CM, Morgan RJ. Structure—Property Relations of Polyethertriamine-Cured Bisphenol-A-diglycidyl Ether Epoxies. In: Bauer RS, editor. Epoxy Resin Chem. II, American Chemical Society; 1983, p. 211–27. doi:10.1021/bk-1983-0221.ch011.

[45] Jones FR. Glass Fibres - Surface Treaments. Handb. Polym. Fibre Compos., Harlow : Longman Scientific & Technical; 1994, p. 46.

[46] Detassis M, Pegoretti A, Migliaresi C. Effect of temperature and strain rate on interfacial shear stress transfer in carbon/epoxy model composites. Compos Sci Technol 1995;53:39–46. doi:10.1016/0266-3538(94)00069-7.

[47] Li C, Potter K, Wisnom MR, Stringer G. In-situ measurement of chemical shrinkage of MY750 epoxy resin by a novel gravimetric method. Compos Sci Technol 2004;64:55–64. doi:10.1016/S0266-3538(03)00199-4.

[48] Hoa S V., Ouellette P, Ngo TD. Determination of Shrinkage and Modulus Development of Thermosetting Resins. J Compos Mater 2009;43:783–803. doi:10.1177/0021998308102035.

Figure Captions

Figure 1. Photo and schematic of microbond test setup

Figure 2. Load-displacement curve for a successful de-bond.

Figure 3. SEM image of de-bonded droplet with meniscus highlighted.

Figure 4. Normalised dimension change versus temperature plot.

Figure 5. Coefficient of thermal expansion above Tg versus amine:epoxy group ratio. Figure 6. Coefficient of thermal expansion below Tg versus amine:epoxy group ratio.

Figure 7. Normalised heat flow versus temperature plot.

Figure 8. Glass transition temperature T_g versus amine:epoxy group ratio plot.

Figure 9. Storage modulus versus temperature ratio plot.

Figure 10. IFSS versus amine:epoxy group ratio plot.

Figure 11. IFSS versus glass transition temperature T_g.

Figure 12. nIR comparison plot of the 2nd derivatives for different R ratios focusing on the downward epoxy group (4530cm^{-1}).

Figure 13. nIR comparison plot of the 2nd derivatives for different R ratios focusing on the downward secondary amine peak (6460 cm^{-1}).

Figure 14. nIR comparison plot of the 2nd derivatives for different R ratios focusing on the downward primary amine peak (4930 cm^{-1}).

Figure 15. Interfacial thermal residual stress contribution τ_R versus amine group: epoxy group ratio.

Figure 16. IFSS versus interfacial thermal residual stress contribution τ_R.

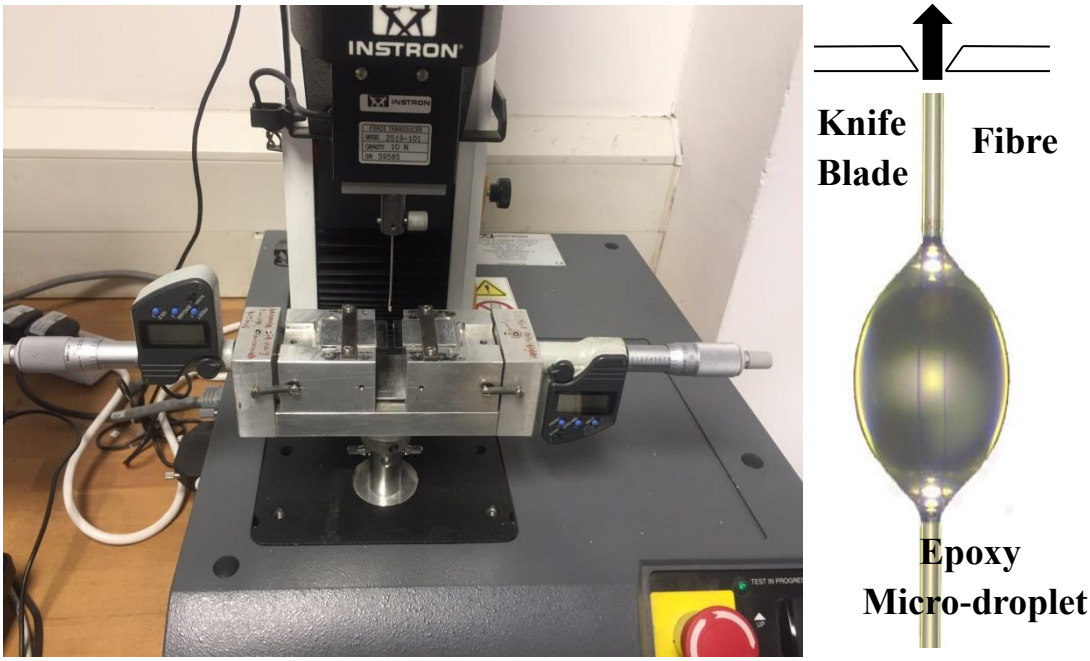

Figure 1. Photo and schematic of microbond test setup.

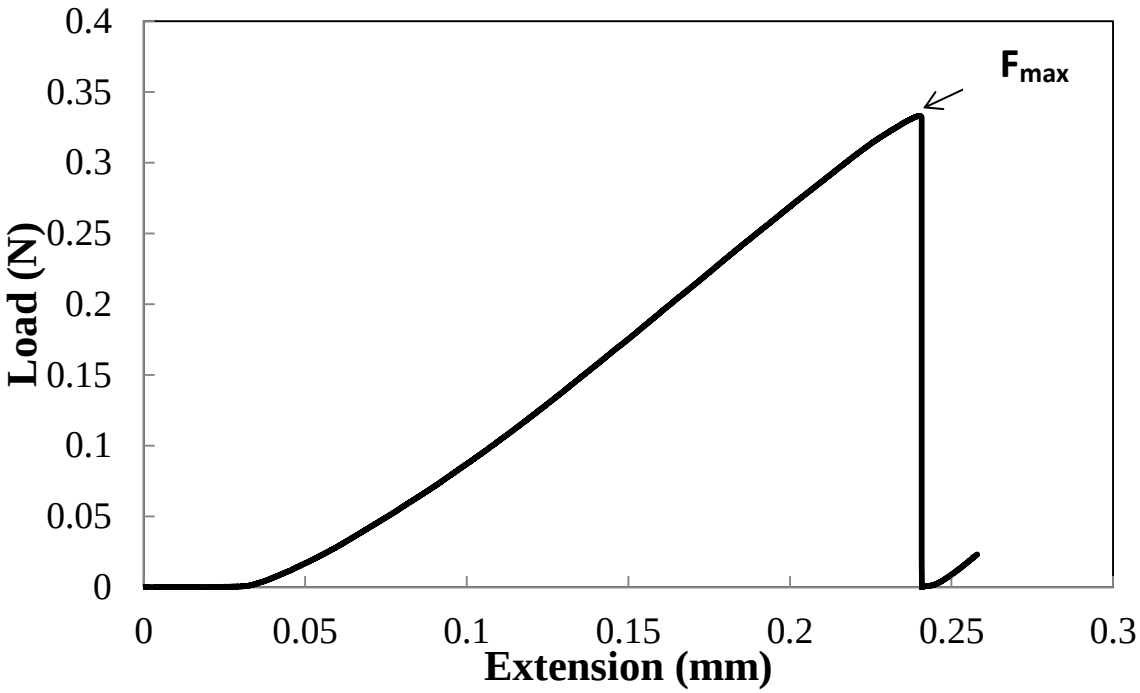

Figure 2. Load-displacement curve for a successful de-bond.

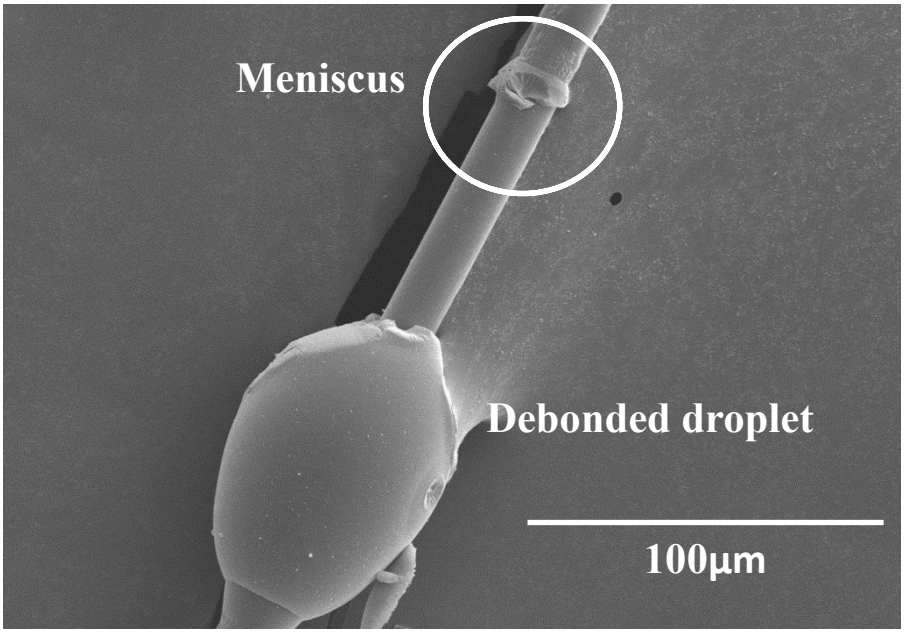

Figure 3. SEM image of debonded droplet with meniscus highlighted.

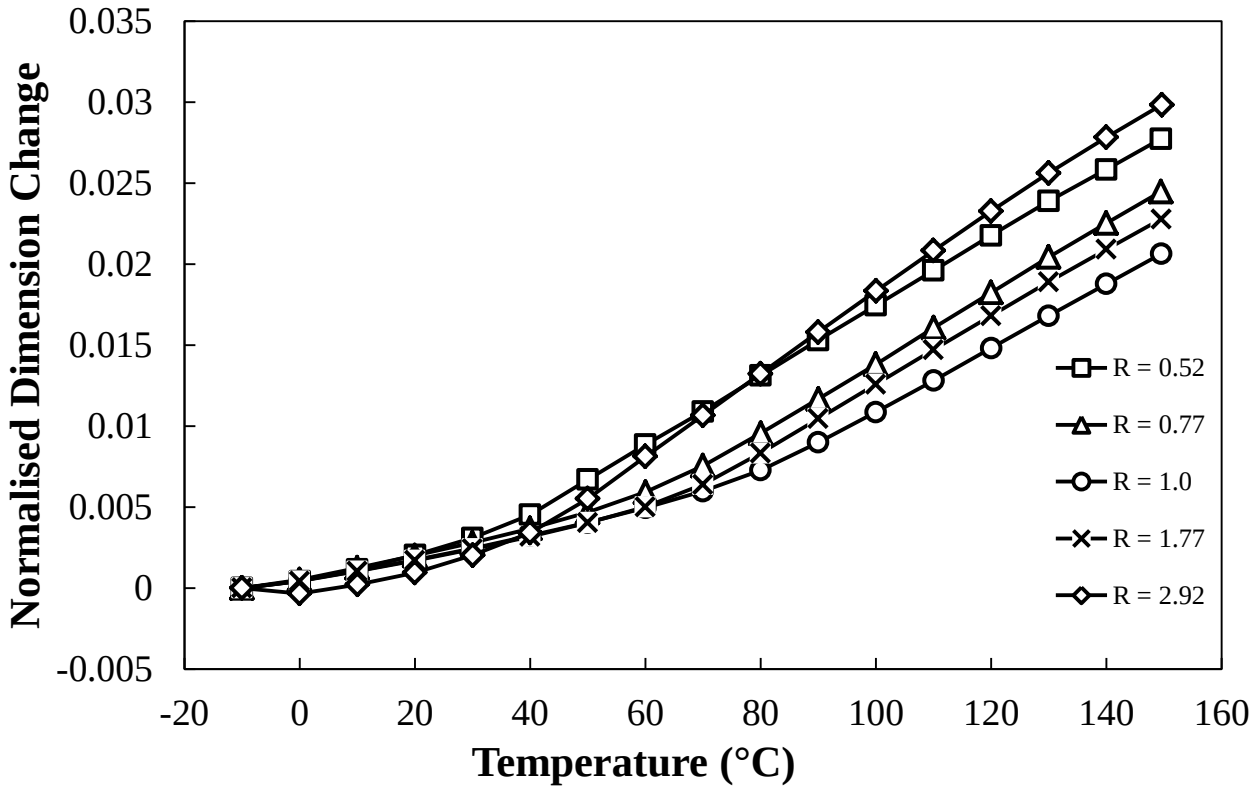

Figure 4. Normalised dimension change versus temperature plot.

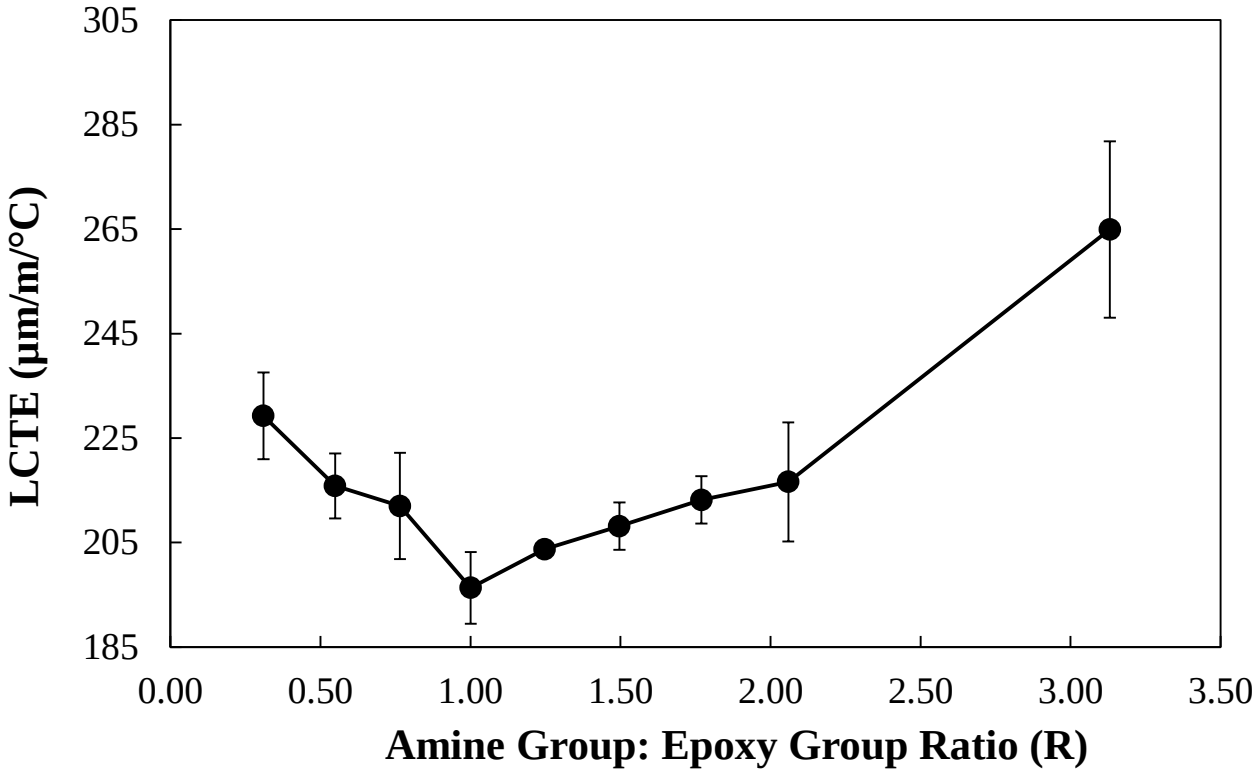

Figure 5. Coefficient of thermal expansion above Tg versus amine:epoxy group ratio.

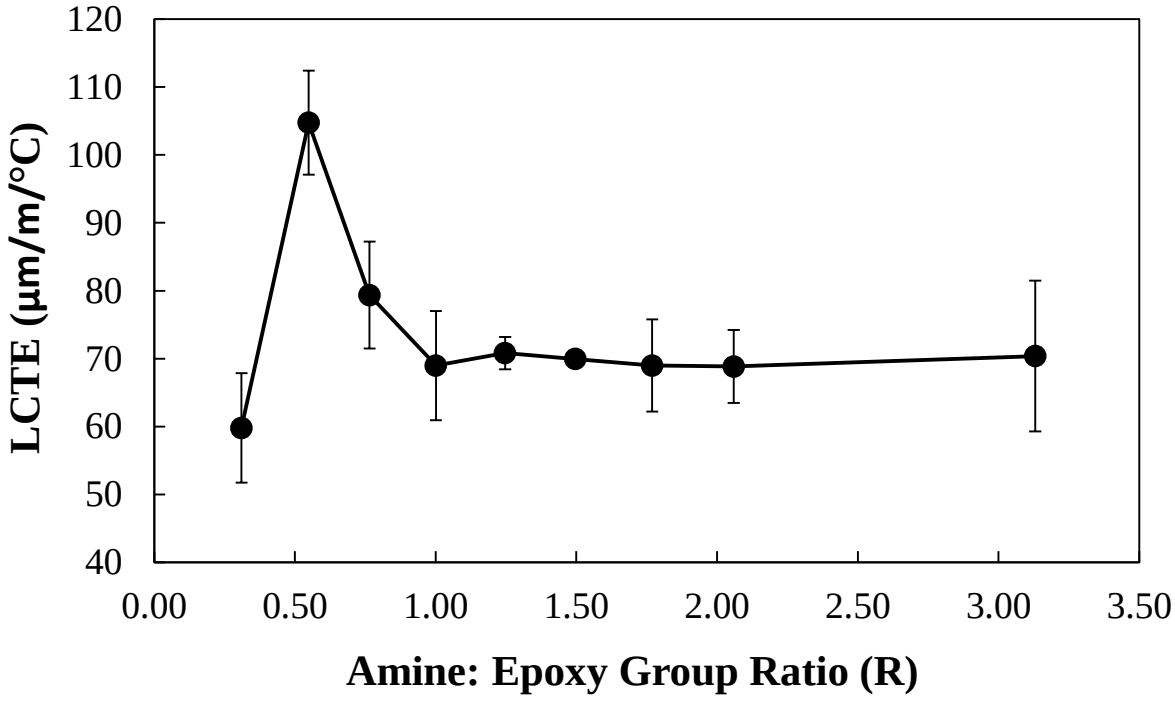

Figure 6. Coefficient of thermal expansion below Tg versus amine:epoxy group ratio.

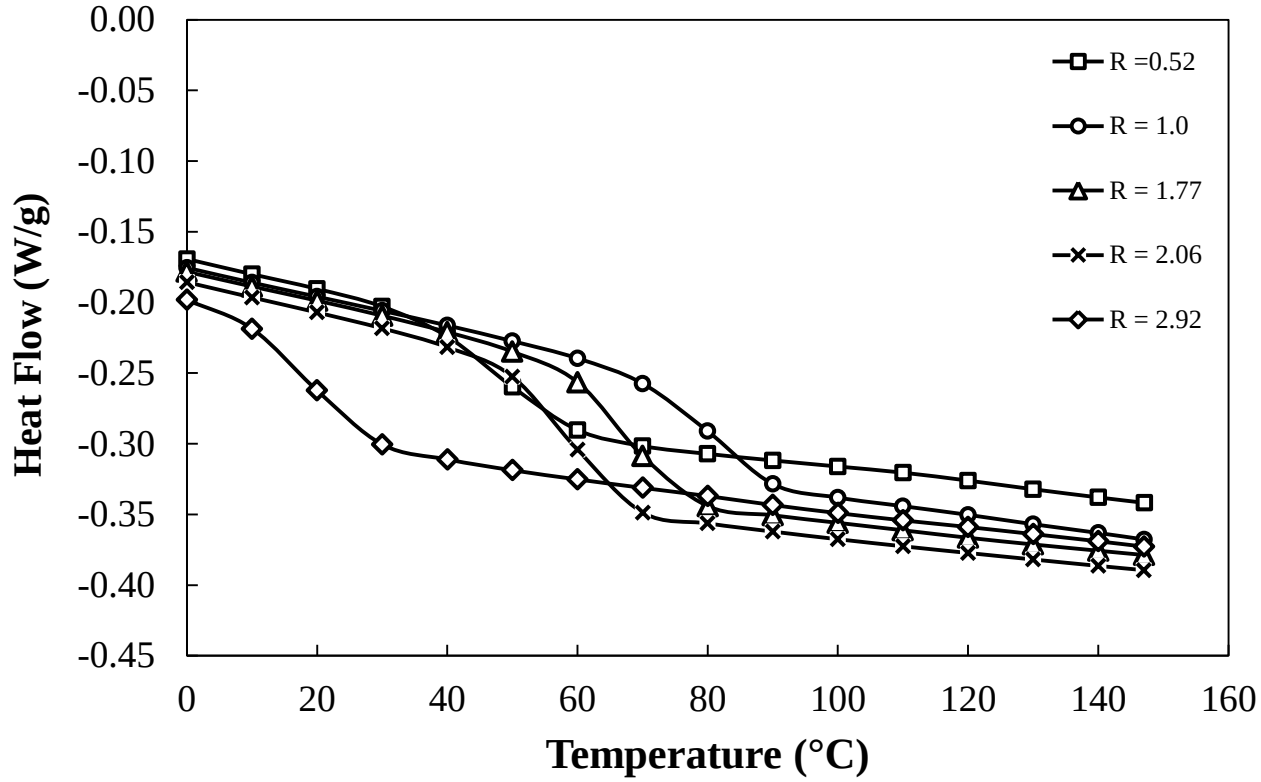

Figure 7. Normalised heat flow versus temperature plot.

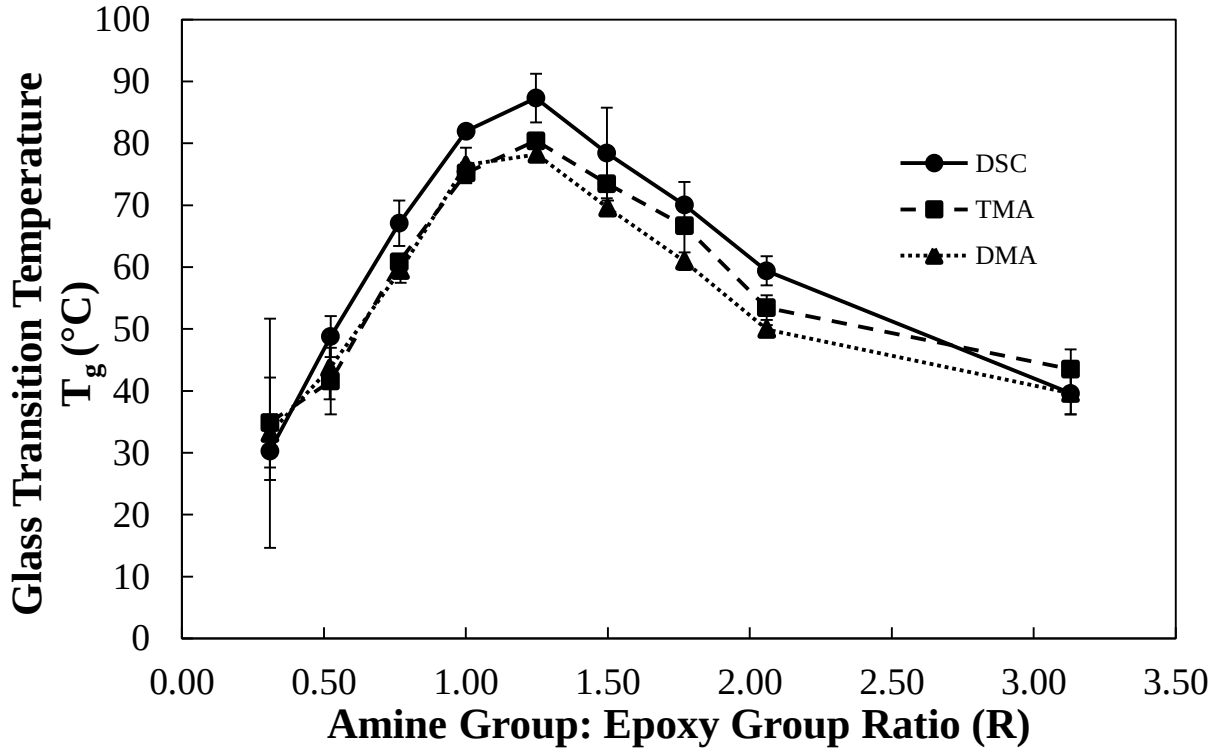

Figure 8. Glass transition temperature T_g versus amine:epoxy group ratio plot.

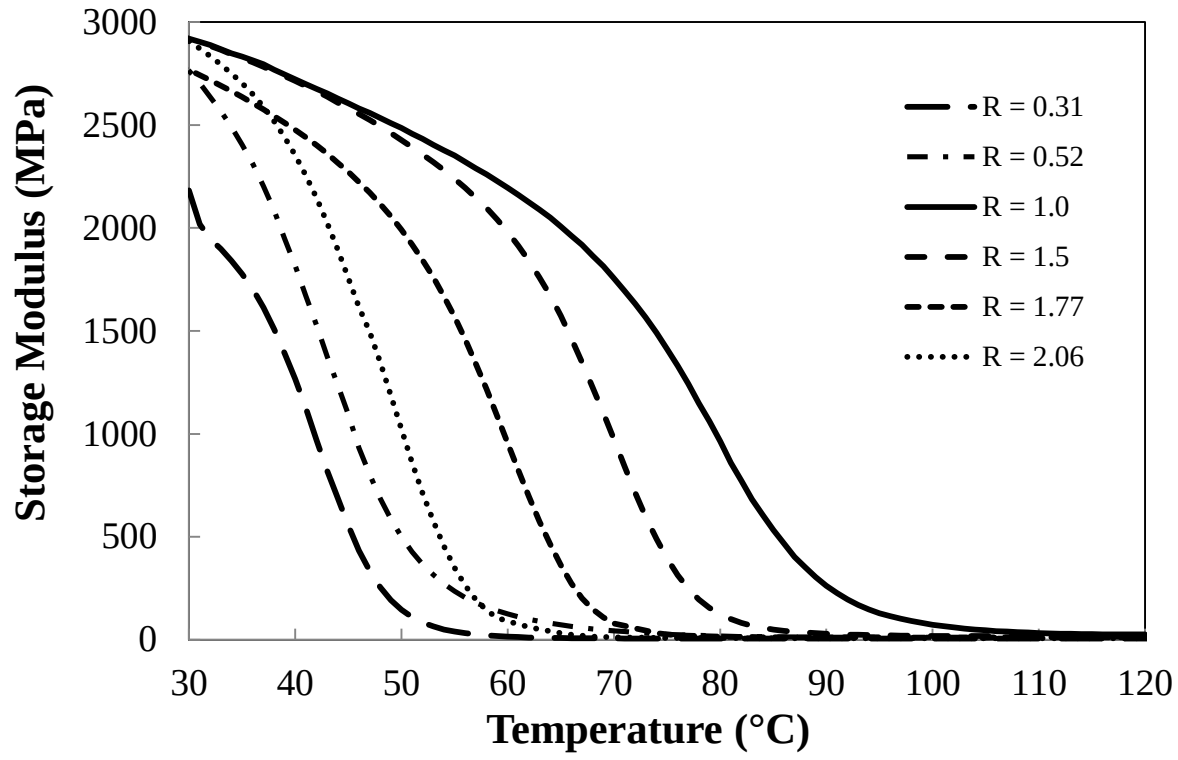

Figure 9. Storage modulus versus temperature ratio plot.

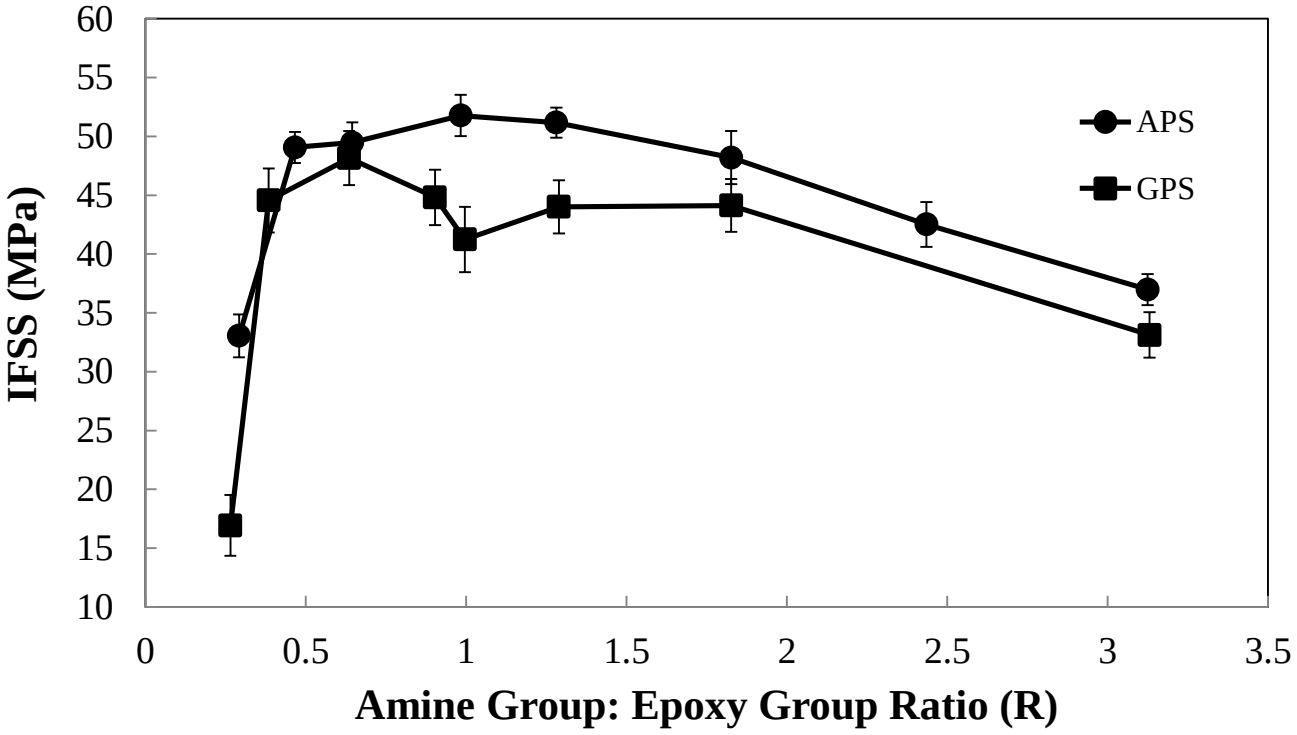

Figure 10. IFSS versus amine:epoxy group ratio for APS and GPS sized fibres.

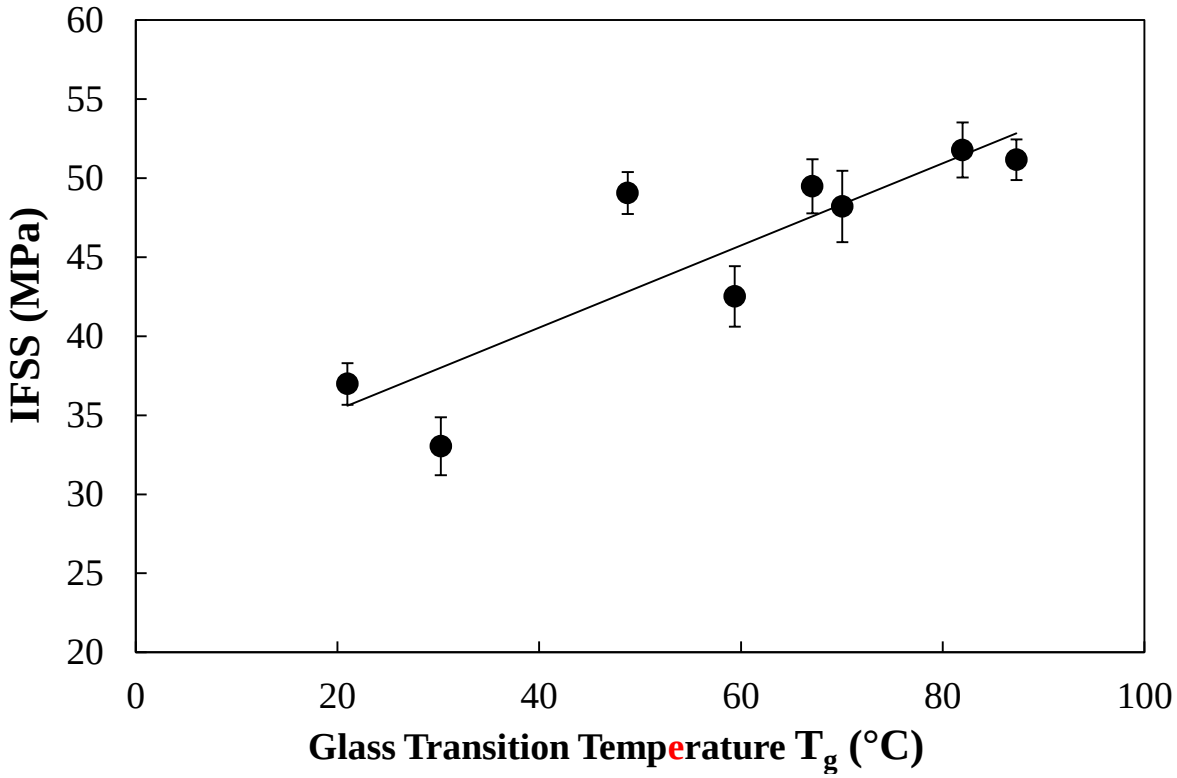

Figure 11. IFSS versus glass transition temperature T_g.

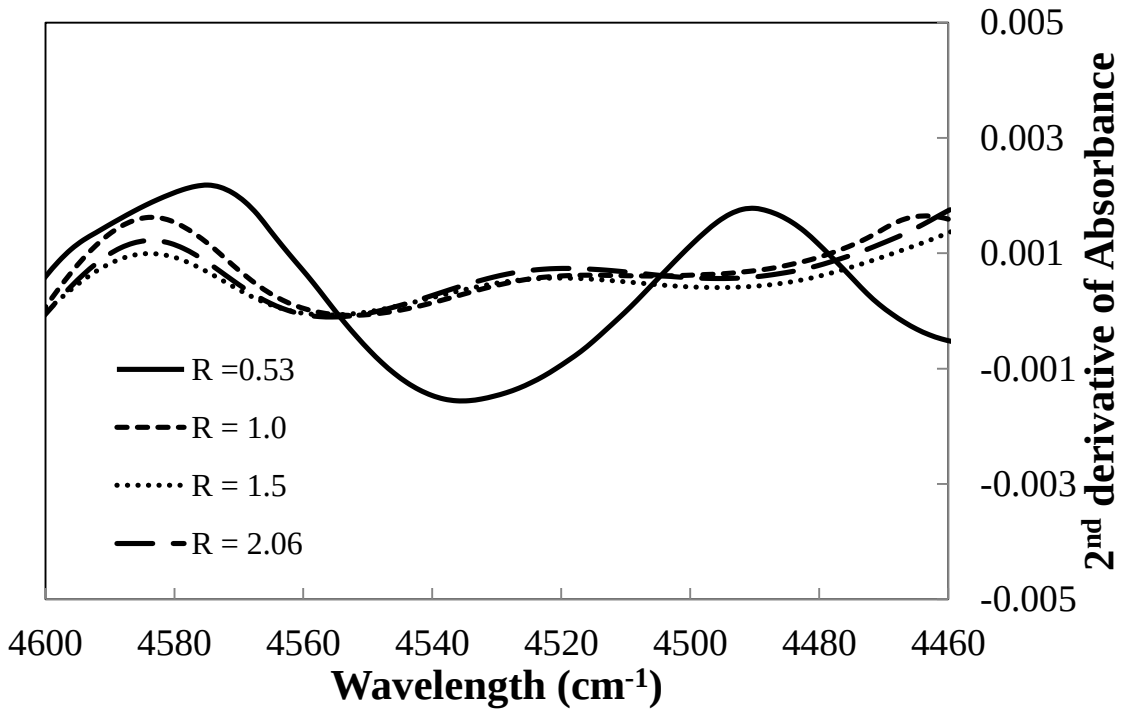

Figure 12. nIR comparison plot of the 2nd derivatives for different R group ratios focusing on the downward epoxy group peak (4530cm^{-1}).

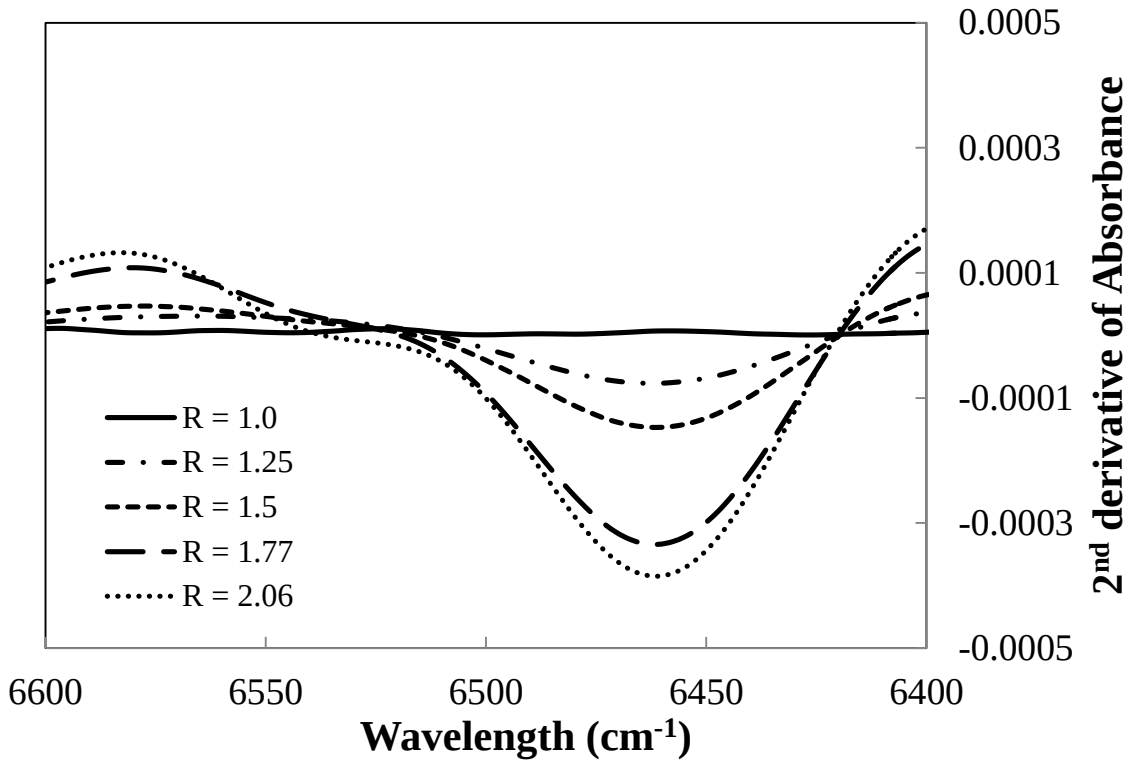

Figure 13. nIR comparison plot of the 2nd derivatives for different R ratios focusing on the downward secondary amine peak (6460 cm^{-1}).

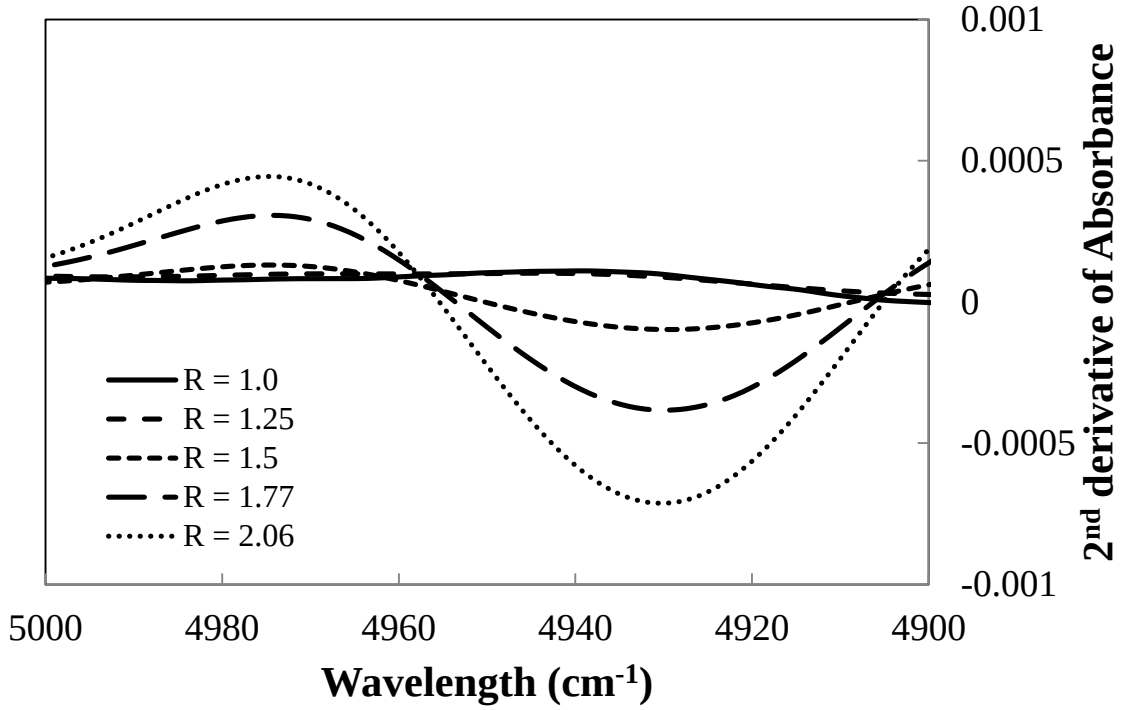

Figure 14. nIR comparison plot of the 2nd derivatives for different R ratios focusing on the downward primary amine peak (4930 cm^{-1}).

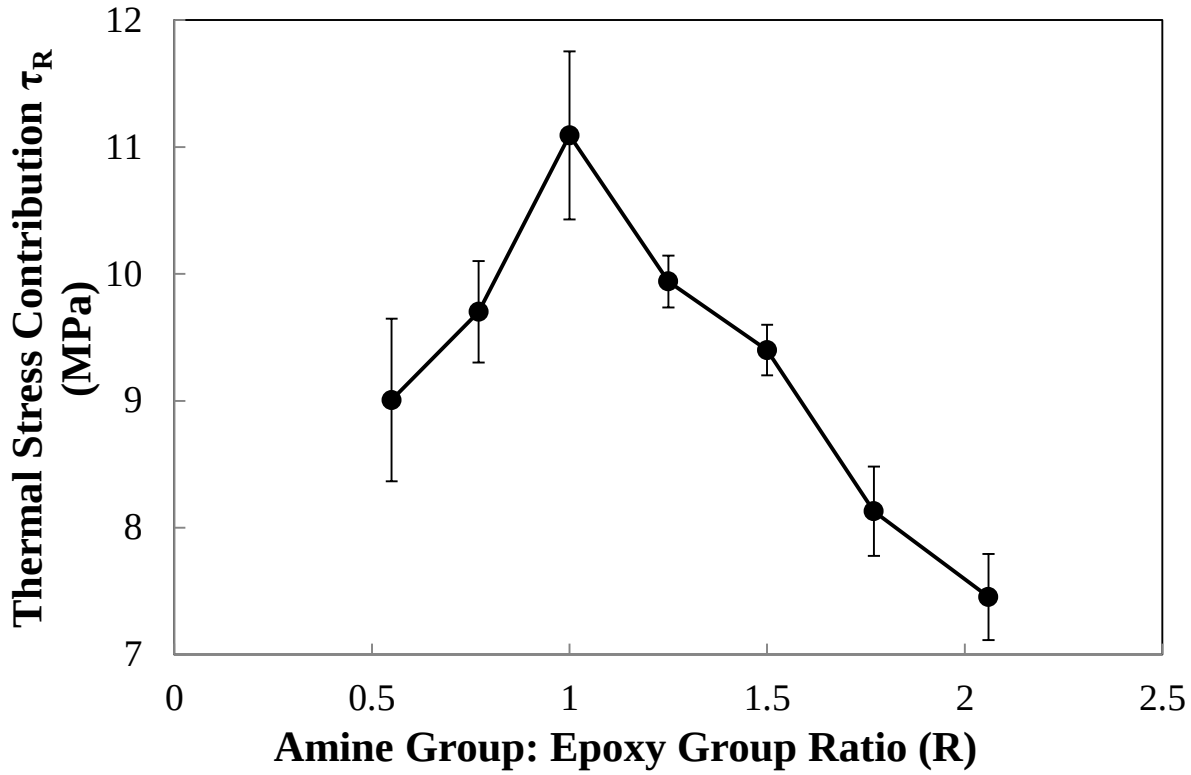

Figure 15. Interfacial thermal residual stress contribution τ_R versus R ratio.

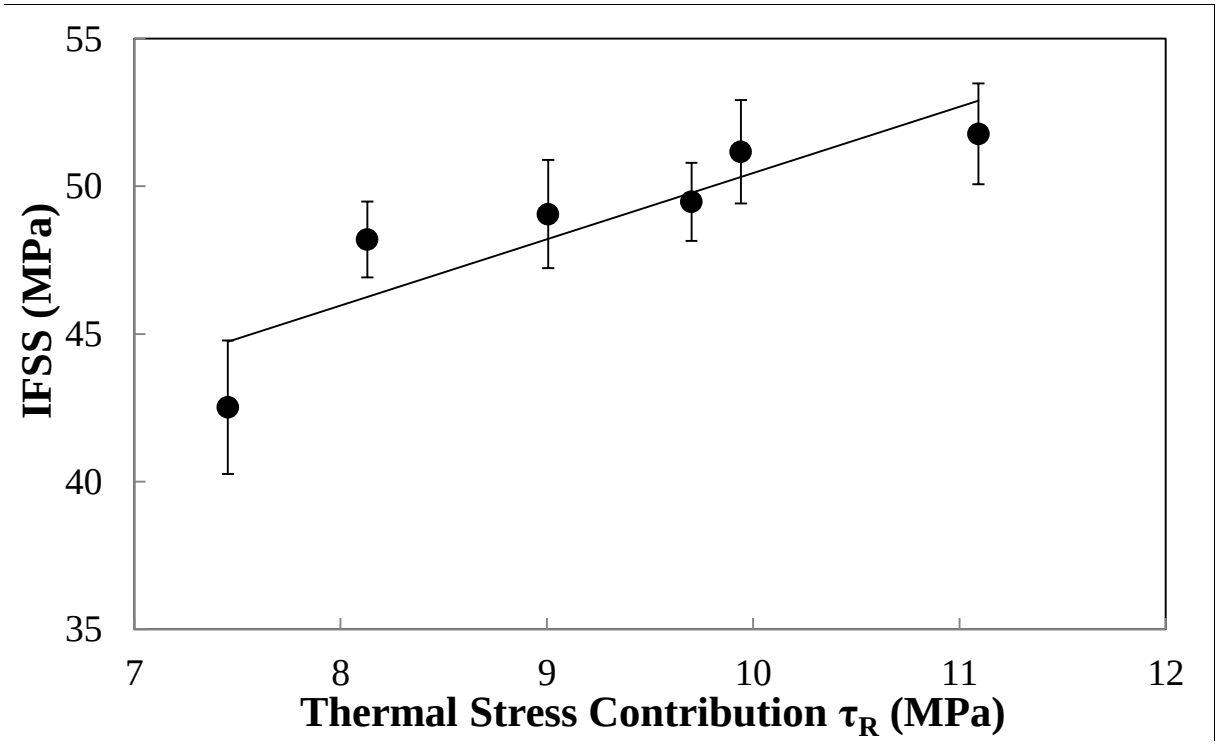

Figure 16. IFSS versus interfacial thermal residual stress contribution τ_R.